AN EXPERIMENTAL INVESTIGATION OF THE FLOW-INDUCED NOISE GENERATED BY A POROUS TRAILING-EDGE OF A FLAT-PLATE

Rahul Sudhakaran[1], Akhilesh Mimani[1], Ric Potreous[1], Con J. Doolan[2]

[1]School of Mechanical Engineering
University of Adelaide, Adelaide SA 5005, Australia
Email: rahul.sudhakaran@student.adelaide.edu.au
akhilesh.mimani@adelaid.edu.au
ric.porteous@adelaide.edu.au

[2]School of Mechanical and Manufacturing Engineering
UNSW, Australia, Sydney NSW 2052, Australia
Email: c.doolan@unsw.edu.au

Abstract

This paper presents the results of an experimental investigation to study the effect of a porous airfoil Trailing-Edge (TE) with different open-area ratios at Reynolds number by 2.9 x $10^5 \leq Re_c \leq$ 4.06 x 10^5 (based on the chord length) and the zero angle of attack ($\alpha = 0$) on the flow-induced noise generation mechanism. Acoustic pressure measurements were taken in an Anechoic Wind Tunnel (AWT) using a spiral array of 31 microphones. Five different TE configurations were considered; these are airfoil with a porous TE modelled by 15, 36, 45 and 72 slits and a reference non-porous plate. A comparison of the Power Spectral Density (PSD) graphs of a porous TE with that obtained due to reference non-porous plate indicates up to 5 dB reduction (on an average) in the noise levels between the frequency range given by 2500 Hz to 8000 Hz due to the use of porous TE. The results obtained from the cross-spectral Conventional Beamforming (CB) algorithm indicate that the noise generation source is closer to the TE at these frequencies. However, in the mid-frequency range between 2000 Hz to 2500 Hz, the noise from the Leading-Edge (LE) is comparable to that observed at the TE. This is hypothesised to be due to the interaction between the LE and the boundary-layer exiting the contraction-outlet.

1. Introduction

Flow-induced noise generated by an airfoil is problematic in the field of aerodynamics and wind energy. In particular, the Trailing-Edge (TE) noise generated due to the interaction of a turbulent boundary-layer with the airfoil is the most significant source of noise caused by the airfoil. According to Howe [1], the TE noise can be reduced by changing its geometry. In another study by Jaworski and Peake [2], it is explained that the TE noise can be reduced with the introduction of poroelasticity. Previous research on noise generation at the TE of porous airfoil primarily focused on homogenous porous materials. The important factor that affects noise generated by the porous airfoil is the airflow resistivity or the surface roughness of the material, see Geyer *et al*. [3]. It was mentioned that porosity and permeability is the dominant feature of an owl's wing that enables it to achieve quiet flight. This feature was employed by

Parchen *et al.* [4] in an airfoil side edge by using a porous material, which in turn reduced the induced drag on airframe as well as the noise generated from the pressure fluctuations at the side edge.

Geyer *et al*. [3] conducted a number of experimental studies based on the measurement of the noise generated at the TE of porous airfoils in uniform flow. They showed from experiments that a noise reduction up to 10 dB was obtained at low-frequency ($f < 4$ KHz) and mid-frequency ($4 \leq f \leq 10$ KHz) for the porous airfoils compared to the non-porous airfoil for medium flow resistivities materials. However, at high-frequencies $(f \geq 10 \text{ kHz})$, the porous airfoil produced higher noise than that of non-porous airfoil. This might be due to the surface roughness of the material [5]. The same trend was followed for material with a low and high flow resistivity, however, the noise reduction obtained for the case of low flow resistivity was less than 5 dB [3].

Angland and Zhang [5] conducted an experimental study on measurements of flow around a flap side-edge with porous edge treatment by adding a porous edge to the half-span flap of a TE to understand its effect on the noise production. The formation of a shear-layer in the flap side-edge was altered due to the porous side-edge, which in turns lead to decrease in the noise created by broadband airframe by displacing the vortices away from the flap surface and changing the pressure distribution over the airfoil. They also conducted a Particle Image Velocimetry (PIV) measurement which indicated that vorticity magnitude in the shear-layer was significantly reduced compared to hard wall and side wall vortices that are displaced away from the surface. Therefore, the reduction of turbulent sources in the shear-layer leads to the generation of weaker noise spectra. Another important observation by Angland and Zhang [5] was that the measurement obtained from the surface microphones indicated the area near the field where the acoustic pressure and particle velocity are not in phase was dominated by the mid-frequency disturbances and a significant change was noticed in the pressure distribution that directly affected the acoustic impedance on the flap side. Thus, the flow field modifications resulting from the porous flap edge showed a significant noise reduction due to changes in acoustic impedance of the porous material.

Poroelastic feature of the owl's wing have also been *analytically* investigated by Jaworski and Peake [2]. An owl's wing was analysed for elasticity and porosity to reduce TE noise for this theoretical study. A study involving a poroelastic-plate model indicated reduced noise levels compared to a flexible brush model developed by Herr [6]. The physical property of materials such as polypropylene, used as part of the flexible brush by Herr [6] was comparable to that of the polyelastic-plate material. Even though the two models were physically different, the former comprised of a flexible material with uniformly separated openings and the latter comprised of polypropylene brush connected to the TE. These two models were compared utilising fibre spacing in which the geometry of the fibres reduced noise and in Herr's model [6], the fibre spacing, diameter and length were less than 1 mm, 0.4 mm and 45 mm, respectively [2]. Thus, the baseline parameters for the poroelastic edge were 0.0014 fractional open-area, 0.026 pore radius, 0.002 was the intrinsic fluid loading parameter (non-dimensionalised by the bending wavelength R), and bending wave Mach number of 0.14 in a vacuum [2]. The fractional open-area was the product of the number of apertures in a poroelastic plate and the area of the holes. The intrinsic fluid loading parameter was the product of the squared Mach number and the fluid loading parameter, where the fluid loading parameter was dependent on properties of the material such as the density, sound speed, frequency and mass. The results from both studies [3, 5] indicated noise reduction at Leading-Edge (LE) for a range of frequencies.

Presently, no work is reported in the literature on an *experimental* investigation of a partially porous airfoil with slits at its TE (that models porous edges) and a non-porous Leading-Edge (LE). This work therefore, presents for the first time, the results of an experimental investigation to study the effect of a porous TE modelled by slits (with different open-area ratios) on reduction in flow-induced noise at low-to-moderate Reynolds numbers ($2.9 \times 10^5 \leq Re_c \leq 4.06 \times 10^5$) for zero angle of attack.

2. Experimental set-up

2.1 Anechoic wind tunnel facility

Experiments were performed in Anechoic Wind Tunnel (AWT) at the University of Adelaide. The internal dimension of the AWT is 1.4 m x 1.4 m x 1.6 m and its walls are acoustically treated with foam

wedges to implement an approximate free-field environment above 250 Hz. The AWT has a rectangular contraction outlet of height 75 mm and width 275 mm that produces a quiet uniform test flow. The maximum free stream velocity of the jet and the turbulence intensity from the contraction-outlet is limited to 38 $\mathrm{m \cdot s^{-1}}$ and 0.33%, respectively, [7-9].

2.2 Equipment and methodology

2.2.1 Measurement equipment

Experiments were conducted at different free-stream velocities given by $U_\infty = \{25,\ 30,\ 35\} \mathrm{m \cdot s^{-1}}$, respectively. The acoustic pressure was recorded for each of the five TEs mounted to the flat-plate (one at a time). As shown in Fig. 1, two side plates were used to mount the flat-plate. Fig. 1 shows that the side plates were flush mounted to the origin of the contraction-outlet at zero angle of attack (α = 0). The position of the LE of the flat-plate was 15 mm downstream of the jet exit planes. The origin is fixed at the opening of the contraction-outlet on its axis as indicated in Fig. 1.

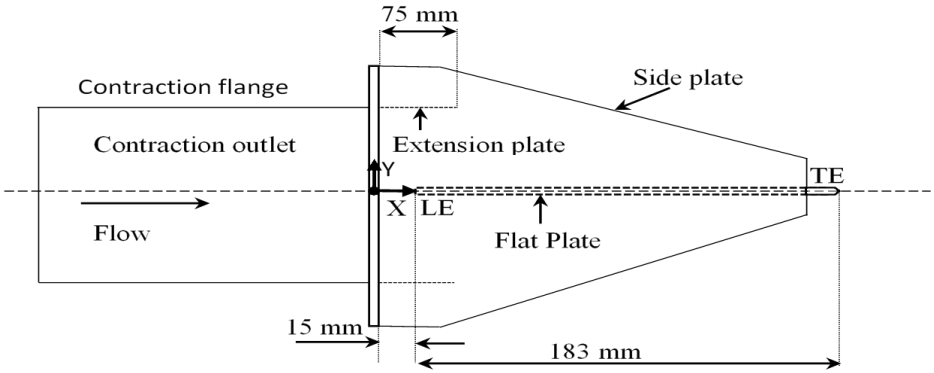

Figure 1. Experimental set-up (side view) along with the flat-plate held between two side plates

A planar microphone array which is parallel to the TE of the flat-plate termed as the top array was used to measure the noise generated by the flat-plate and was located 530 mm above it. The top array design consists of 31 GRAS 40PH ¼ phase-matched microphone, see Fig. 2. A pattern developed by Underbink was used to irregularly space the microphones to avoid spatial problem and spatial aliasing inside the AWT.

Figure 2. Top spiral array of microphones used to measure acoustic pressure signals

2.2.2 Data processing procedure

The acoustic pressure was recorded at 31 microphones of the spiral array and stored in the hard-drive using a National Instruments PXI-8016 data acquisition system containing 4 PXI-4496 simultaneous sample and hold ADC cards. Microphone data was acquired at a sampling frequency $f_s = 2^{16}$ Hz for a sampling time of 40 s and presented in narrow band with a frequency resolution of 64 Hz. A Power

Spectral Density (PSD) versus frequency plot was generated using Welch's function with a Hanning window of length 65536 samples each, and a 50 % overlap. Simultaneously, a cross-spectral matrix was calculated using a Conventional Beamforming (CB) algorithm from the experimental data recorded by the microphones to obtain the one third-octave band source maps that describes the distribution of sound strength and location over the test-area.

2.3 Test models

The test model is a flat-plate with chord length $C_L = 183$ mm which consists of two parts, a main steel body and a detachable TE made from thin aluminium sheets. The TE with different porous design and serrations can be attached to the main body by changing the detachable TE. The thickness and the span of the main body were 6 mm and 450 mm, respectively (see Fig. 3).

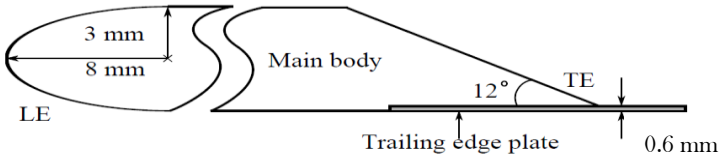

Figure 3. Diagram of Flat-plate model [7, 8]

The TE was asymmetrically bevelled at an angle of 12° to the main body [7]. The TE plates was attached to the main body with 24 M2 x 0.4 screws. Five TEs with a thickness of 0.6 mm were used in this experiment and the specifications of each TE are discussed below.

2.3.1 Reference plate

The reference plate is made of a thin non-porous aluminium sheet with a span of 450 mm and width of 105 mm (see Fig. 4). The wetted surface area of the reference plate is different from TEs with pores.

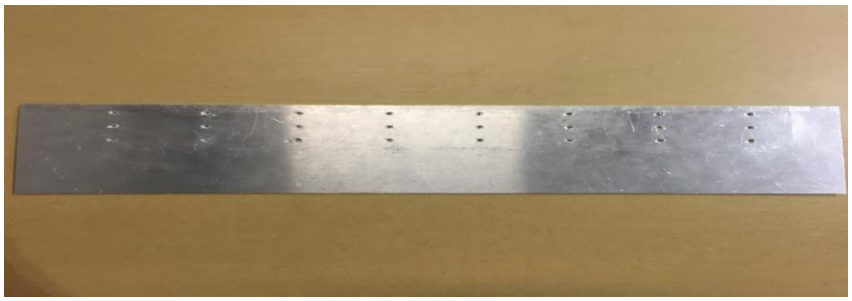

Figure 4. Reference plate TE

2.3.2 Trailing edge numbers 15, 36, 45 and 72

In this work, slits were chosen to simulate TE porosity rather than holes [3] as the turbulence in the boundary-layer of the holes impinge on the downstream back surface and create additional noise. However, in the case of silts, due to the absence of downstream back surface, excess noise is not generated, thereby ensuring that the slits are ideally suited to model the porous TE. The porosity of the TE is determined using the open-area ratio of the plate, which is defined using the equation 1 where H= 30 mm, L = 450 mm and h =15 mm are constant.

$$\propto_h = \frac{N \times h \times t}{H \times L}. \quad (1)$$

Equation (1) was used to determine the number of slits or divisions that is required for a particular open-area ratio with a given spacing t between each slits, see Table 1. The breadth of the plate that is exposed to the flow is represented by H while L is the span of the TE and h is the amplitude of the slit. The values for open-area ratio and spacing were chosen from the theoretical study conducted by Jaworski and Peake [2]. However, the exact values used by Jaworski and Peake [2] for their theoretical study was

not implemented for this experiment due to manufacturing constrains. Therefore, using trial and error, the following open-ratio values given by 0.05, 0.08, 0.05 and 0.08 and the corresponding spacing given by 1, 3, 2 and 1 mm, respectively, are used to obtain 15, 36, 45 and 72 slits, respectively, see Fig. 5. A thin aluminium sheet was used to manufacture the TEs with determined number of slits.

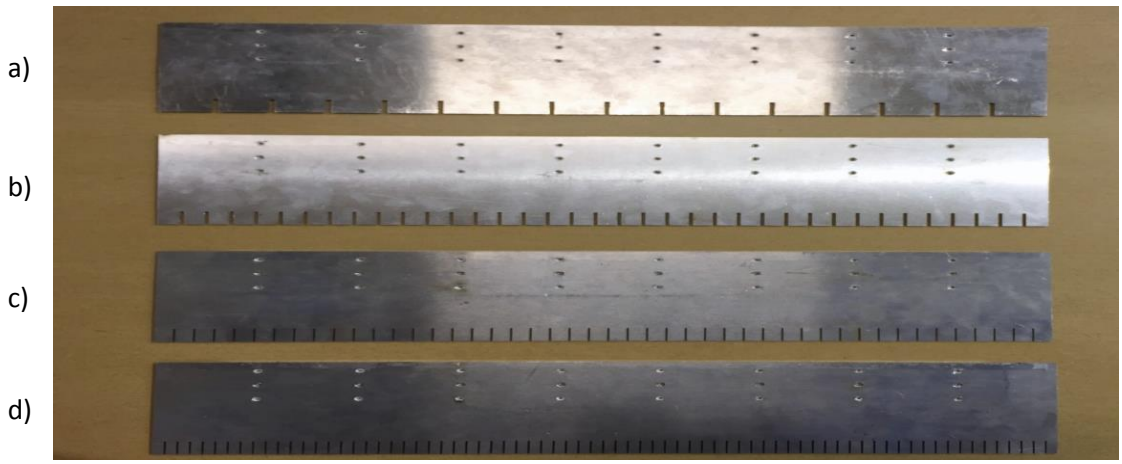

Figure 5. Porous plate TE with thickness t = 6 mm and number of slits N = (a) 15, (b) 36, (c) 45 and (d) 72.

Table 1. Test matrix

Serial Number	Open-Area Ratio	Number Of Division (N)	Spacing (mm)
1	0.05	45	1
2	0.08	72	1
3	0.05	15	3
4	0.08	36	2

3. Experimental results

3.1 Acoustic spectra

3.1.1 Effect of porous trailing-edge in the acoustic spectra

Figures 6-8 show the acoustic spectra for the reference plate and the four porous plates for a free stream velocity, U_∞ for $U_\infty = 25\ \mathrm{m.s^{-1}}, 30\ \mathrm{m.s^{-1}}$ and $35\ \mathrm{m.s^{-1}}$, respectively. The legend N used in the PSD graphs indicates the number of slits. Figures 6-8 illustrate that the slits were effective in reducing the noise generated by the TE across a wide range of frequencies. When the number of slits is increased, noise reduction up to 5 dB is obtained in the mid-Strouhal number range given by $0.064 \leq St \leq 0.18$, (on an average) where the TE noise was dominant. However, at a higher Strouhal number, slits were not effective, indicating that at high-frequency, porous TE produces slightly more noise than that of non-porous TE. It is noted that $f < 3150\ Hz$ is the low-frequency, $3150\ Hz \leq f \leq 9000\ Hz$ is the mid-frequency region and $f > 9000\ Hz$ is the high-frequency. The associated Strouhal number (St) with respect to the TE thickness is defined using the equation 2.

$$St = \frac{f \times t_{TE}}{U_\infty}, \tag{2}$$

where f is the frequency, U_∞ is the free stream velocity and t_{TE} is the TE thickness.

For $25\ \mathrm{m.s^{-1}}$ the corresponding Strouhal number region for the low frequency is $St < 0.075$, mid-frequency range is $0.075 \leq St \leq 0.21$ and high-frequency range is $St > 0.21$. Similarly the corresponding low, mid and high frequencies for $30\ \mathrm{m.s^{-1}}$ are $St < 0.063$, $0.063 \leq St \leq 0.18$, $St > 0.18$

and for 35 m. s^{-1} are $St < 0.054$, $0.054 \leq St \leq 0.15$, $St > 0.15$.

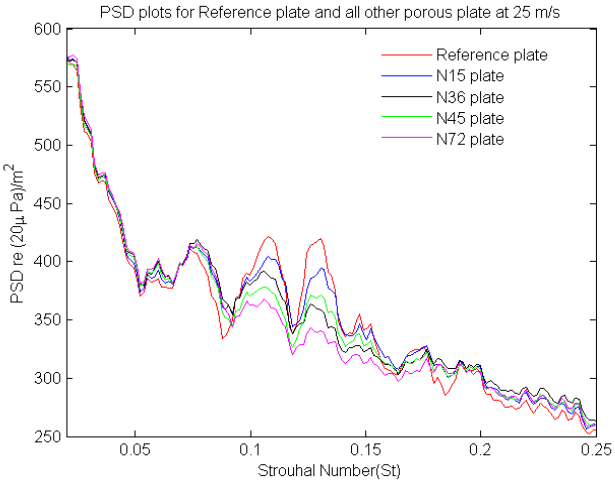

Figure 6. PSD plot for reference plate and all other porous plate at 25 m. s^{-1}

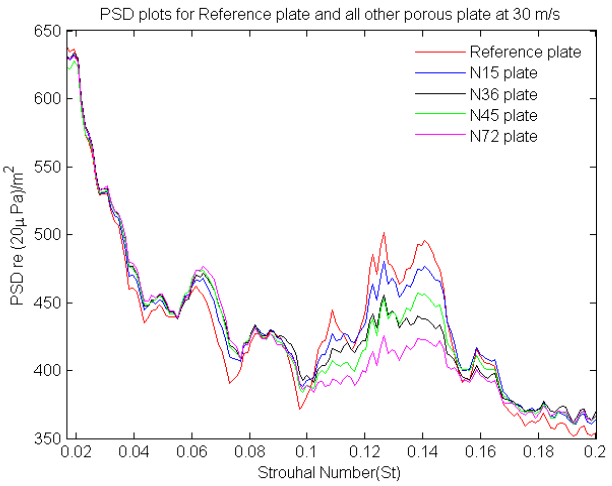

Figure 7. PSD plot for reference plate and all other porous plate at 30 m. s^{-1}

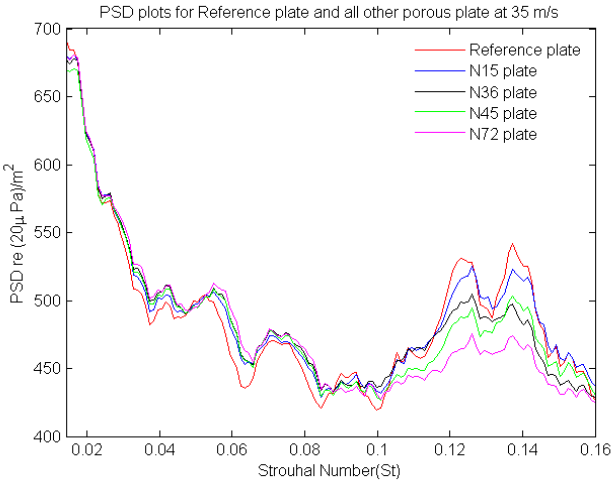

Figure 8. PSD plot for reference plate and all other porous plate at 35 m. s^{-1}

It is important to note that since the wetted surface area of the TE of the four different porous TE configurations and the reference plate are *unequal*, their respective PSD graphs were divided by the wetted surface area of the respective flat-plate. As a result, the PSD per meter square was plotted against Strouhal number based on the boundary-layer thickness of the TE.

Table 2 shows the average area under the graph of PSD/m^2 versus Strouhal number where the noise was dominant for the reference plate and the four porous plate by using the trapezoidal numerical integration method.

Table 2. Noise reduction comparison for reference plate and the porous TE plate

TE plate	At 25 m. s^{-1}		At 30 m. s^{-1}		At 35 $m. s^{-1}$	
	Area between $St = 0.07 - 0.11 -$	Noise reduction w.r.t the reference plate (in dB)	Area between $St = 0.10 - 0.12$	Noise reduction w.r.t the reference plate (in dB)	Area between $St = 0.11 - 0.12$	Noise reduction w.r.t the reference plate (in dB)
Reference plate	393.78	0	479.92	0	522.90	0
N 15	381.53	1	464.97	1.2	511.60	1
N 36	365.95	2.29	437.44	3.4	486.88	3
N 45	362.01	2.6	443.95	2.9	492.41	2.5
N 72	346.28	4	416.07	5.3	466.29	4.7

3.2 Beamforming source maps

Figures 9(a-h) show the CB source maps obtained using the top spiral array of planar microphones located above the TE for the *reference plate* at 30 $m \cdot s^{-1}$. The CB source maps are presented in one-third octave band centre frequencies from 1600-8000 Hz. (It is noted that the source maps are not shown in lower one-third octave bands due to poor resolution.)

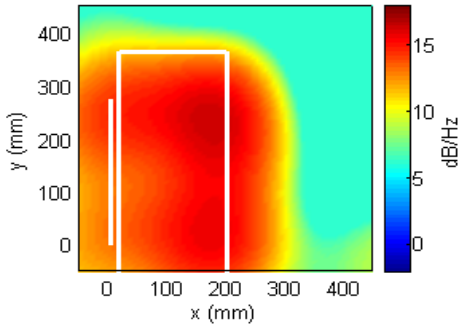

(a) 1600 Hz (*St* = 0.032)

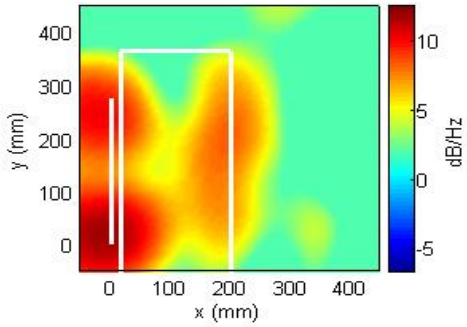

(b) 2000 Hz (*St* = 0.04)

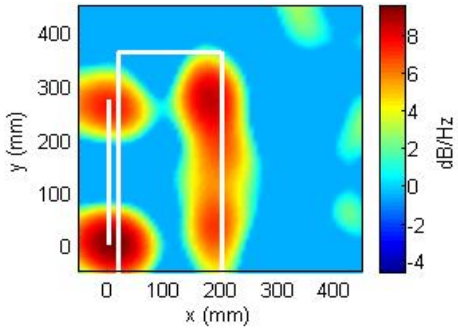

(c) 2500 Hz (*St* = 0.05)

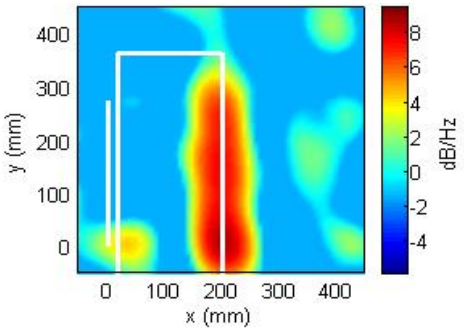

(d) 3150 Hz (*St* = 0.063)

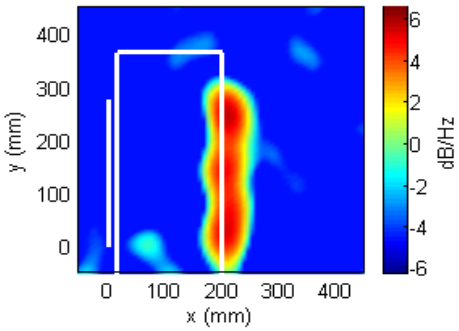

(e) 4000 Hz (*St* = 0.08)

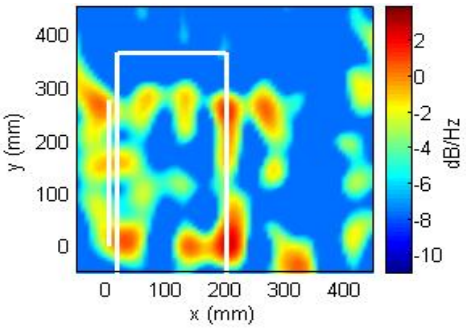

(f) 5000 Hz (*St* = 0.01)

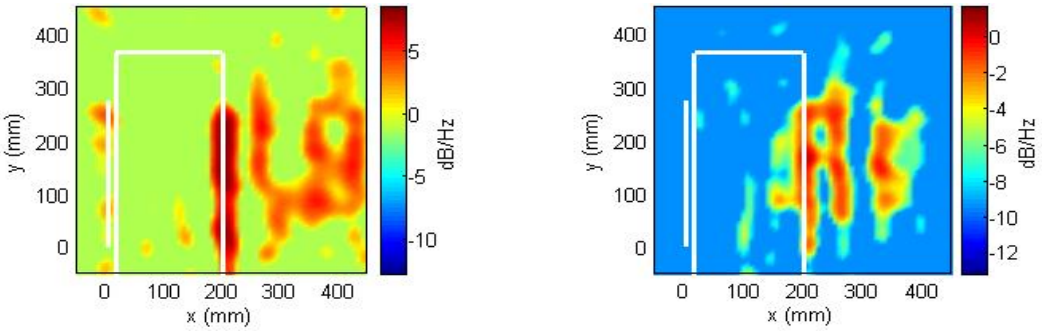

(g) 6300 Hz (St = 0.126) (h) 8000 Hz (St = 0.16)

Figure 9. CB source maps for reference plate at 30 m. s^{-1} for center band frequency between 1600-8000 Hz

The mean flow is taken along the positive x direction (left to right, see Fig. 9) for all the CB source maps presented in this paper. The vertical straight line indicates the contraction-outlet, the rectangular box indicates reference flat-plate and the rectangular box with one dotted side indicates the porous flat-plate. (The same symbolic conventions are followed in the remaining results shown in this paper.) A shear-layer correction factor of 4 mm was applied to the beamforming images based on the equation (3), where X_s is the shear-layer correction factor, M is the Mach number and k is the contraction-outlet length.

$$X_s = M \times \frac{k}{2} \tag{3}$$

Blake [10] shows that if $f > c_0/C_l$ (where c_0 is the speed of sound and C_l is the chord length) then the TE noise will be separated from the LE noise. In this work, for $f > 1874.3$ Hz, the TE noise generated by the flat-plate is independent of the LE noise. Figures 9(d-h) indicate that above 2500 Hz, the noise generated by the TE is dominant noise source, especially in the high-frequency range [9]. The TE noise region spread from mid-span to the tip of the flat-plate. Additionally, the CB source maps also show the magnitude of noise generated by the flat-plate.Qualitatively, similar results also obtained in different one-third octave bands for porous edges N = 15, 36, 45 and 72, however, these are not shown for brevity.

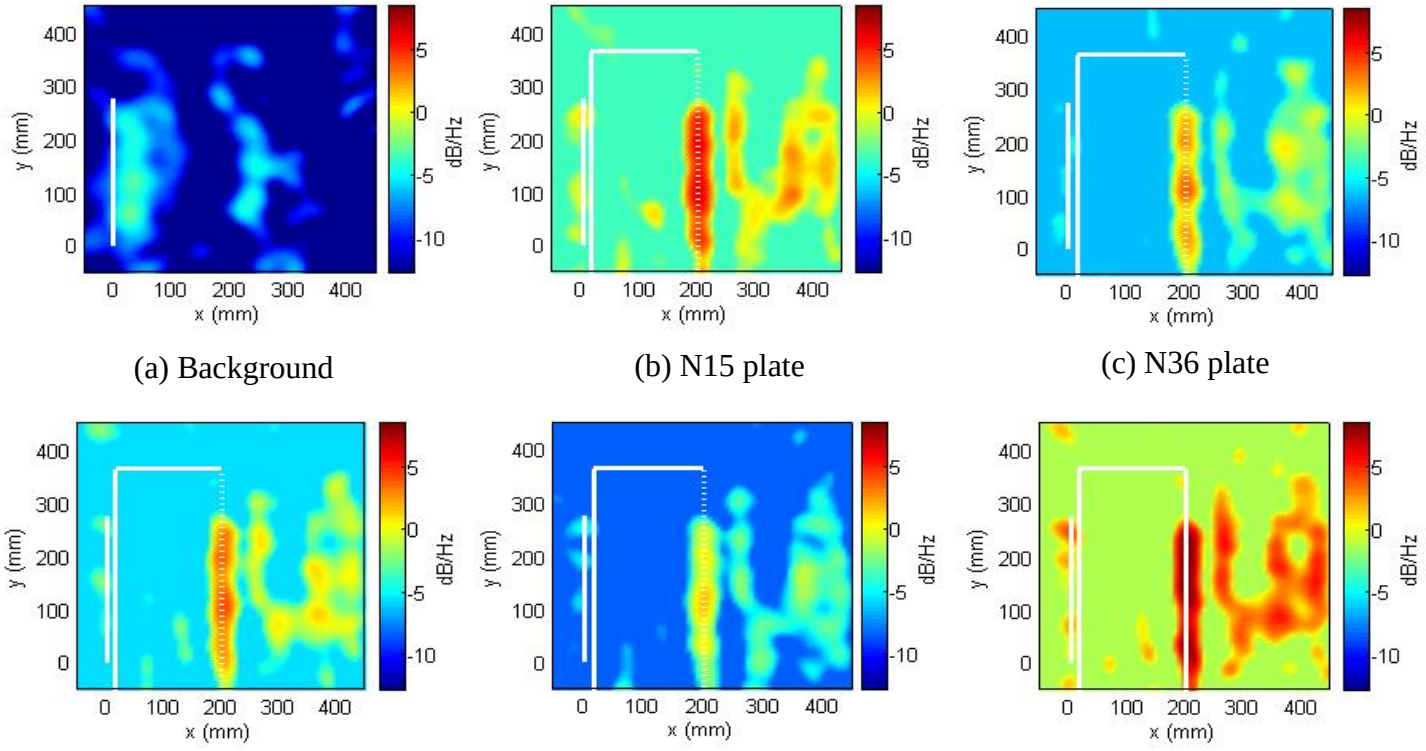

(a) Background (b) N15 plate (c) N36 plate

(d) N45 plate (e) N72 plate (f) Reference plate

Figure 10. Sound Maps for background noise, reference plate and four different porous for 6300 Hz (St = 0.126) at 30 m. s^{-1}

Figure 10(a–f) show the CB source maps for background noise, reference plate and four other porous TE plates at a centre band frequency of 6300 Hz (St = 0.126) where maximum noise reduction is achieved by slit plates (with respect to reference plate) at $U_\infty = 30\ \mathrm{m \cdot s^{-1}}$.

Figure 10 indicates the main lobes accompanied by side-lobes are located at the TE of the flat-plate. The colour bar located on the right side of the source map indicates the magnitude of noise generated by the TE wherein it is observed that the reference plate produces maximum noise in this particular one-third octave band and the noise level decreases as the number of slits in the TE increases. Similar results were also obtained for mean flow speeds given by 25 and 35 $\mathrm{m.\,s^{-1}}$, not shown for brevity. Furthermore, the side-lobes can be thought of as imperfections in the CB source maps which are caused due to the point spread function. The deconvolution techniques such as DAMAS or CLEAN-SC may be used to reduce the side-lobe levels.

3.2 Spatial integration

In order to quantify the individual contribution of the LE and TE noise sources to the overall radiated far-field acoustic pressure field, spatial integration of the acoustic pressure field (obtained from the CB source map) is carried out over a small rectangular region enclosing the LE and TE (shown in Fig. 11) yielding the average Sound Pressure Level (SPL) of the acoustic sources in the particular frequency band of interest. It is noted that Fig. 11 represents the CB source map for reference plate at 30 $\mathrm{m.\,s^{-1}}$. The two rectangular boxes shown using dotted sides indicates the area of integration and its length and breadth are given by 104 mm and 273 mm, respectively.

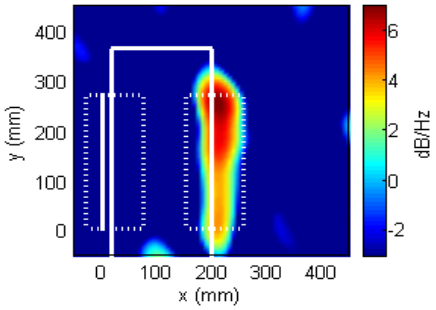

Figure 11. CB source map (for a reference plate at centre band frequency 4000 HZ at 30 $\mathrm{m.\,s^{-1}}$) showing the spatial integration area represented by rectangles

Figure 12 show the spatial integration graph for reference and four porous flat-plate at 30 $\mathrm{m.\,s^{-1}}$.

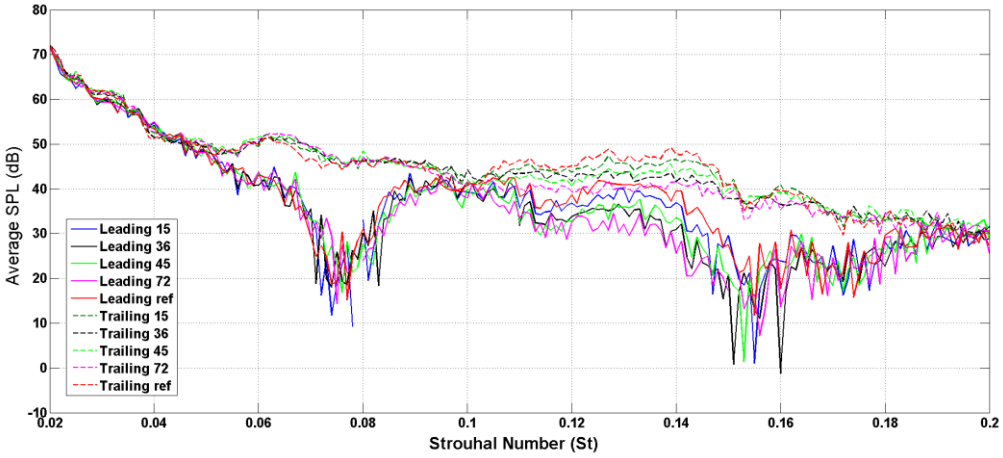

Figure 12. PSD spectra for the specific region around the LE and TE of the reference and porous TE flat-plate at a free stream velocity $U_\infty = 30\ m.s^{-1}$

The spatial integration graph shows that the noise created by the flat-plate is due to the TE of the flat-plate, especially in the high-frequency range [9]. The PSD plot shows the noise generation for the overall porous TE flat-plate, however, it is difficult to individually distinguish LE and TE sources from

it. The spatial integration graphs shown in Fig. 12 enables one to individually quantify the noise generated by the LE and the TE. Importantly, from the spatial integration graph, it is evident that noise was generated at the TE for the test models, which implies that it is the porous TE that reduces the noise by about 5 dB (on an average) in the mid Strouhal number range from $0.064 \leq St \leq 0.18$.

An another interesting feature observed from the Fig. 12 is that when the TE noise reduces with the increase of slits, a similar pattern is observed in the LE of the flat-plate which needs to be further investigated for understanding the reason for the decrease of LE noise. It is noted that spatial integration graph for 25 $\mathrm{m.s^{-1}}$ and 35 $\mathrm{m.s^{-1}}$ follow a similar trend as that shown in Fig. 12, hence, these are not shown here.

4. Conclusion

This paper has presented the results of an experimental investigation that studied the effect of a porous Trailing-Edge (TE) with different open-area ratios at low-to-moderate Reynolds number range given by 2.9 x $10^5 \leq \mathrm{Re_c} \leq$ 4.06 x 10^5 (based on the chord length) and the zero angle of attack on the flow-induced noise generation mechanism. It is shown that with an increase in the number of slits, the porous TE minimises the noise up to 5 dB in the mid Strouhal number range from $0.064 \leq St \leq 0.18$. However, at high Strouhal number range, the porous TE produces slightly more noise than that generated by the non-porous TE. Furthermore, the source maps obtained by Conventional Beamforming (CB) as well as the spatial integration graphs indicate that the noise sources generated by the flat-plate are located at the TE especially in the high-frequency range [9] with exception of the one-third octave band centred at 2000 Hz (i.e., at St = 0.04) wherein the LE generates more noise than that generated by the TE.

Acknowledgements

The first author acknowledges the support of School of Mechanical Engineering, The University of Adelaide.

References

[1] Howe, M. "Noise produced by a sawtooth trailing edge", *Journal of the Acoustical Society of America*, **90**, 482-487, (1991).

[2] Jaworski, J.W. and Peake, N. "Aerodynamic noise from a poroelastic edge with implications for the silent flight of owls", *Journal of Fluid Mechanics*, **723**, 456-479, (2013).

[3] Geyer, T., Sarradj, E. and Fritzsche, C. "Measurement of the noise generation at the trailing edge of porous airfoils," *Experiments in Fluids*, **48**, 291-308, (2010).

[4] Parchen, R., Hoffmans, W., Gordner, A. and Braun, K. "Reduction of airfoil self-noise at low Mach number with a serrated trailing edge", 6th *International Congress on Sound and Vibration*, Copenhagen, Denmark, 5-8 July 1999, pp. 3433-3440.

[5] Angland, D., Zhang, X. and Molin, N. "Measurements of flow around a flap side edge with porous edge treatment", *AIAA Journal*, **47**, 1660-1671, (2009).

[6] Herr, M. "Design criteria for low-noise trailing edges", *13th AIAA/CEAS Aeroacoustics Conference*, Rome, Italy, 21-23 May 2007.

[7] Moreau, D. J, Brooks, L. A and Doolan, C. J. "Broadband trailing edge noise from a sharp-edged strut", *Journal of the Acoustical Society of America*, **129**, 2820-2829, (2011).

[8] Moreau, D. J and Doolan, C. J. "Noise-reduction mechanism of a flat-plate serrated trailing edge", *AIAA Journal*, **51**, 2513-2522, (2013).

[9] Mimani, A., Moreau, D. J. and Doolan, C. J. "Experimental application of aeroacoustic time-reversal", *21st AIAA/CEAS Aeroacoustics Conference*, Dallas, USA, 22-26 June 2015.

[10] Blake, W. *Mechanics of Flow Induced Sound and Vibration*: *Complex flow-structure interactions*, Academic Press, New York, 1986.